Available online at www.sciencedirect.com
ScienceDirect
Physics of the Earth and Planetary Interiors 157 (2006) 181–187
PHYSICS OF THE EARTH AND PLANETARY INTERIORS
www.elsevier.com/locate/pepi

Elasticity of Mg_2SiO_4 ringwoodite at mantle conditions

Li Li [a,b,*], Donald J. Weidner [a,b], John Brodholt [a], Dario Alfè [a], G. David Price [a]

[a] *Department of Earth Sciences, University College London, Gower Street, London WC1E6BT, UK*
[b] *Mineral Physics Institute, Department of Geosciences, University of New York at Stony Brook, Stony Brook, NY 11790, USA*

Received 31 January 2006; received in revised form 14 March 2006; accepted 5 April 2006

Abstract

The themoelastic properties of Mg_2SiO_4 ringwoodite at mantle pressure and temperature conditions are reported based on ab initio molecular dynamic simulations. A third-order Birch–Murnaghan equation at a reference temperature of 2000 K is defined by $K_0 = 138$ GPa, $K_0' = 5.2$, and $V_0(2000\,\mathrm{K}) = 560.3\,\text{Å}^3$. The Grűneisen parameter is determined to be $\gamma(V) = \gamma_0(V/V_0(298\,\mathrm{K}))^q$ with $\gamma_0 = 1.22$ and $q = 1.44(5)$, with $V_0(298\,\mathrm{K}) = 524.56\,\text{Å}^3$. The thermal expansion is determined to be $(\alpha/\alpha_0) = (V/V_0(298\,\mathrm{K}))^{\delta_T}$ in which $\alpha_0 = 2.74 \times 10^{-5}\,\mathrm{K}^{-1}$ and $\delta_T = 5.2(1)$. The bulk modulus is temperature independent at constant volume, while the shear moduli vary with temperature at constant volume. Elastic anisotropy decreases with both pressure and temperature becoming isotropic by the bottom of the upper mantle.

Keywords: Ringwoodite; Elasticity; First principle; Molecular dynamics; High pressure and high temperature

1. Introduction

Ringwoodite is the most abundant mineral in the Earth's transition zone between the 520 and 660 discontinuities (Anderson and Bass, 1986). The elastic properties of ringwoodite are of primary interest for understanding the transition zone structure and dynamics (Duffy and Anderson, 1989). The elastic anisotropy of this mineral is also crucial in understanding the seismic anisotropy in the deep mantle (Fischer and Wiens, 1996; Karato, 1998). The elastic properties of ringwoodite have been studied extensively both experimentally and theoretically, but in a limited pressure (P) and temperature (T) range. Reported ultrasonic data (Li, 2003; Rigden et al., 1991) give both shear and longitudinal sound velocity at high P but at room T. Brillouin spectroscopy has been used to measure single crystal elastic moduli at either room P–room T (Sasaki et al., 1982; Weidner et al., 1984); or high P–room T and high T–room P (Jackson et al., 2000; Sinogeikin et al., 2001, 2003), none of which reached mantle P–T conditions. Stress measurements of ringwoodite in the diamond-anvil cell (Kavner, 2003; Kavner and Duffy, 2001) were conducted at room T with a clear goal of identifying the elastic anisotropy but are possibly contaminated by the presence of plastic anisotropy (Weidner et al., 2004). The equation of state of ringwoodite was determined at both high P and T (up to 700 K) (Meng et al., 1993) using an externally heated diamond anvil cell but with a lack of information on elastic anisotropy and at relatively low T compared with mantle conditions. Despite the large number of experimental data, there is still a lack of information of the elasticity of this phase at mantle P–T. Theoretically calculated elastic properties have also been reported. Elastic properties of ringwoodite at

* Corresponding author. Tel.: +1 631 632 8220; fax: +1 631 632 8140.
E-mail address: Lilli@ic.sunysb.edu (L. Li).

0031-9201/$ – see front matter © 2006 Elsevier B.V. All rights reserved.
doi:10.1016/j.pepi.2006.04.002

$T = 0$ K were calculated using the plane-wave pseudopotential method up to 30 GPa (Kiefer et al., 1997). Elastic properties at high P–T were calculated using molecular dynamic (MD) simulations with a Breathing shell model (BSM) (Matsui, 1999) which depends on an empirical pair potential. Recent publications (Oganov et al., 2001a,b; Stackhouse et al., 2004) have shown that the ab initio molecular dynamics (AIMD) method is powerful for predicting the thermoelastic properties of silicate minerals (e.g. $MgSiO_3$ perovskite) at mantle P–T conditions. We apply the same methodology to calculate the thermoelasticity of Mg_2SiO_4 ringwoodite. We present a complete equation of state which allows the calculation of sound velocities in the mantle P–T range. Our results indicate a quasi harmonic approximation would bias the shear modulus in this temperature range. We find that ringwoodite is nearly isotropic throughout its region of stability in the mantle.

2. Methodology

The elastic constants of Mg_2SiO_4 ringwoodite were calculated using ab initio molecular dynamics (AIMD) simulations with the VASP code (Kresse and Furthmüller, 1996). We used the projector-augmented-wave (PAW) (Blöchl, 1994; Kresse and Joubert, 1999) implementation of density functional theory (DFT) and the implementation of an efficient extrapolation for the charge density (Alfè, 1999). All calculations were performed using a 56-atom unit-cell. A plane-wave cut-off energy 500 eV was used. Increasing the plane-wave cut-off to 600 eV caused the value of the elastic constants to change by an average of 0.5 percent. The Γ point was used for sampling the Brillouin zone. The time step used in the dynamical simulation was 1 fs. The core radii are 2.0 a.u. for Mg (core configuration $1s^2 2s^2$), 1.9 a.u. for Si ($1s^2 2s^2 2p^6$) and 1.52 a.u. for O ($1s^2$). The equilibrium structure was obtained after the stresses on three principle axis are equal (within ±0.5 GPa) and the off-diagonal stresses are zero. The convergence of the stresses on each axis is carefully checked to be within ±0.5 GPa. The computation time to reach equilibration varies among configurations. It depends on the starting atom positions, vibration velocities and temperature. It took at least 2 ps calculation to reach the equilibrium. Applying positive and negative strains (1%, 1.5% and 2.5%) to the equilibrated structure, stresses were averaged values over 1 ps simulation. Tests show that the effect of longer simulation on the calculated results is small. The linearity between stress and strain was carefully checked for the strains applied. A primary test of stress calculation using a 112-atom cell with box size of $1 \times 1 \times 2$ or $1 \times \sqrt{2} \times \sqrt{2}$ give identical results on the principle and off-diagonal stresses within ±0.5 GPa, which is of the same order of the statistical error, indicating that an increase of box size by a fact of two has little effect on calculated results. The acoustic velocities as a function of crystallographic direction were derived from the calculated single-crystal elastic constants using the Christoffel equation (Nye, 1957).

3. Elastic constants at 0 K

A 56-atom cell with $Fd3m$ atom positions was used in these calculations. We defined the relaxed atom positions and calculated the elastic constants at 0 K and room pressure which we can compare with the reported results (Kiefer et al., 1997; Weidner et al., 1984) as listed in Table 1. Our results are consistent with the experimental results of the previous study (Weidner et al., 1984) as are the reported calculations (Kiefer et al., 1997). The differences among the two calculations are to be expected owing to the different exchange-correlation potential used. Our 0 K elastic constants are slightly larger than the experimental data (largest 6% for c_{12}) which is expected since the experimental temperature is 300 K.

It is well known that the GGA model tends to overestimate the pressure when compared with experiments. We have taken an approach to define, empirically, a pressure off-set between the calculated pressure and the measured pressure for a given volume (Li et al., submitted for publication; Oganov et al., 2001b). This presumes that the calculations provide the correct physical property as a function of volume and temperature. We corrected the

Table 1
Comparisons of elastic moduli, c_{ij}; bulk modulus, K; shear modulus, μ; sound velocities, V_P and V_S; anisotropy $A = 2c_{44}/(c_{11} - c_{12})$ among theoretical results (at $T = 0$ K) and experimental measurement ($T = 300$ K)

c_{11} (GPa)	c_{12} (GPa)	c_{44} (GPa)	K (GPa)	μ (GPa)	V_P (km s^{-1})	V_S (km s^{-1})	A	References
361	118	134	199	129	10.08	5.94	1.10	Kiefer et al. (1997)
327	112	126	184	119	9.79	5.77	1.17	Weidner et al. (1984)
315	106	127	176	118	9.83	5.85	1.21	This study

K and μ are calculated as Voigt–Reuss–Hill averages.

Table 2
Calculated c_{ij}, K, μ, A, V_P and V_S at P_c and T

P_c (GPa)	V (Å^3)	T (K)	c_{11} (GPa)	c_{12} (GPa)	c_{44} (GPa)	K (GPa)	μ (GPa)	A	V_P (km s^{-1})	V_Φ (km s^{-1})	V_S (km s^{-1})
−5.3	539.67	0	315	106	127	176	118	1.21	9.83	7.15	5.85
14.2	493.04	0	422	168	128	253	128	1.01	10.59	8.19	5.82
5.3	512.00	0	376	140	127	219	123	1.08	10.27	7.76	5.82
22.1(2)	493.04	1500	428	176	130	260	128	1.03	10.69	8.30	5.83
13.3(3)	512.00	1500	357	149	122	219	115	1.17	10.11	7.76	5.62
24.7(3)	493.04	2000	408	177	124	254	121	1.08	10.49	8.20	5.66
15.9(3)	512.00	2000	365	135	116	207	111	1.01	10.05	7.64	5.65
29.8(4)	493.04	3000	409	181	113	257	113	0.99	10.40	8.26	5.47
21.0(3)	512.00	3000	353	148	105	217	104	1.03	9.89	7.72	5.36

P_c is the corrected pressure $P_c = P - 5.3$ GPa. Error analysis for the pressures was performed by reblocking the data, as described for examples elsewhere (Allen and Tildesley, 1997). Elastic constants are within 10% error.

pressure by combining our bulk modulus (K)–volume (V) relationship with the experimental volume (V_0). We fitted our V–K data at 0 K using a Birch Murnaghan equation of state with a reference room temperature volume $V_0 = 524.56$ Å^3 (Sasaki et al., 1982), we derived $K_0 = 198$ GPa and $K' = 4.07$. With this equation of state, we calculated the pressure at the investigated volumes. The three 0 K data yield a consistent 5.3(±0.1) GPa offset, supporting our assumption of a constant pressure offset. Our previous studies have shown that this offset is insensitive to temperature as well (Li et al., submitted for publication). In the following text, we used corrected pressure (P_c) to represent the pressure term, $P_c = P - 5.3$ GPa where P is the pressure calculated by VASP for the model volume and temperature.

4. Thermoelastic parameters and *P–V–T* equation of state

The goal of this study is to calculate the P–V–T equation of states and elastic moduli of Mg_2SiO_4 ringwoodite at mantle P–T. We performed our simulations at three temperatures: 1500, 2000 and 3000 K and two volumes (493.04 and 512.00 Å^3). Table 2 lists the calculated results. Fig. 1 illustrates the dependence of the elastic moduli on temperature at each volume. The calculated single crystal elastic modulus c_{11} decreases with temperature at fixed volume, the largest gradient $(\partial c_{11}/\partial T)_V = -0.01$ GPa K^{-1} at $V = 493.04$ Å^3, while c_{12} increases with temperature yielding a nearly constant bulk modulus, K, as a function of temperature with fixed volume. The shear modulus, c_{44}, demonstrates the strongest temperature dependence at constant volume of all of the elastic moduli with values around $(\partial c_{44}/\partial T)_V = -0.012$ GPa K^{-1}. The shear modulus, c_s also decreases with temperature, but at a much slower rate than c_{44} yielding a decreasing deviation from isotropy with increasing temperature. As shown in Fig. 2 the bulk modulus $K = (c_{11} + 2c_{12})/3$ is independent of temperature at constant volume within the uncertainty of the calculation, while the shear modulus (Voigt–Reuss–Hill average), G, decreases with temperature at constant volume indicating anharmonic contributions to the shear modulus.

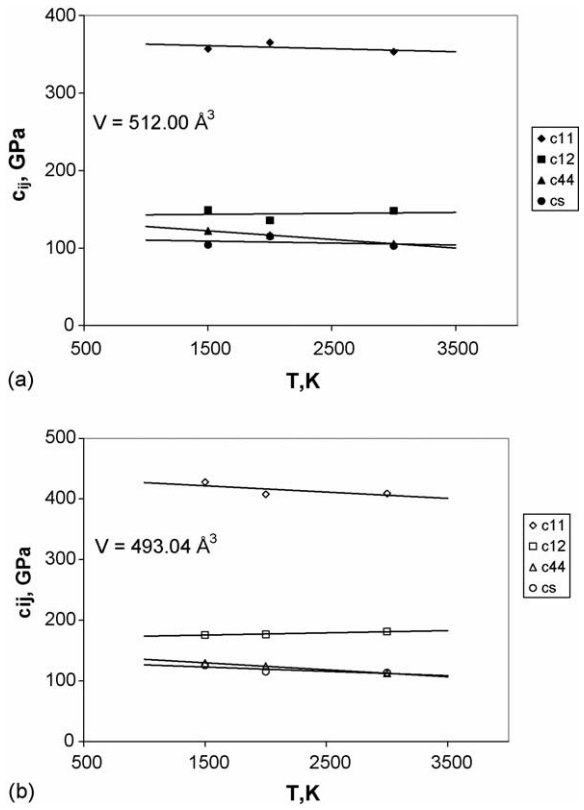

Fig. 1. Elastic moduli c_{ij} vs. temperature T for: (a) $V = 512.00$ Å^3, (b) $V = 493.04$ Å^3. Anisotropy (A) is given by the ratio of c_{44} and c_s. For both volumes, A converges to 1. At low temperature, A is the greatest for the lower pressure.

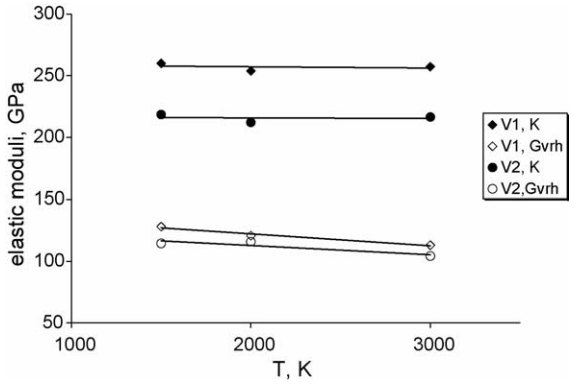

Fig. 2. Elastic moduli vs. temperature (T) at two volumes ($V_1 = 512.00$ and $V_2 = 493.04$ Å^3). The bulk moduli (K) are temperature independent at fixed volumes, while Reuss–Voigt–Hill average shear modulus (G_{VRH}) decrease with temperature at the two calculated volumes. The temperature derivative of shear modulus $\partial G/\partial T(V = 493.04\ \text{Å}^3) = 9.7 \times 10^{-3}$ GPa K^{-1}; $\partial G/\partial T(V = 512.00\ \text{Å}^3) = 7.5 \times 10^{-3}$ GPa K^{-1}.

The comparison between the calculated bulk modulus, K, and experimental values are plotted in Fig. 3. The experimental data are at either room temperature or high pressure (symbol SS) or at elevated temperature and room pressure (symbol JJ). All data are plotted as a function of V/V_0 where $V_0 = 524.56$ Å^3 (Sasaki et al., 1982). The theoretical calculations agree very well with the experimental observations; supporting the quasi-harmonic contention that bulk modulus depends only on volume.

The thermal parameters are calculated and listed in Table 3. Thermal expansion α is obtained from $(\partial P/\partial T)_V/K_T$. Since the bulk modulus K_T appears to be insensitive to temperature at constant volume within the error of calculated pressure (as listed in Table 2), the thermal expansion also becomes temperature insensitive at constant volume in the calculated P–T conditions. The Grűneisen parameter, $\gamma(V)$, is calculated from the thermal pressure and thermal energy: $\gamma(V) = P_{th}(V, T)V/E_{th}(V, T)$, where the thermal energy $E_{th} = 3(N-1)k_bT$, with k_b is the Boltzmann constant, N is the number of atoms in the supercell, $N = 56$ in this study. Fitting the relation: $\gamma = \gamma_0(V/V_0)^q$, we obtain $\gamma_0 = 1.22$ and $q = 1.44 \pm 0.05$. The Anderson Grűneisen parameter, δ_T, is given by $\delta_T = (\partial \ln \alpha/\partial \ln V)_T$. Our best-fit values are $\delta_T = 5.2 \pm 0.05$ and $\alpha_0 = 2.74 \times 10^{-5}$ K^{-1}.

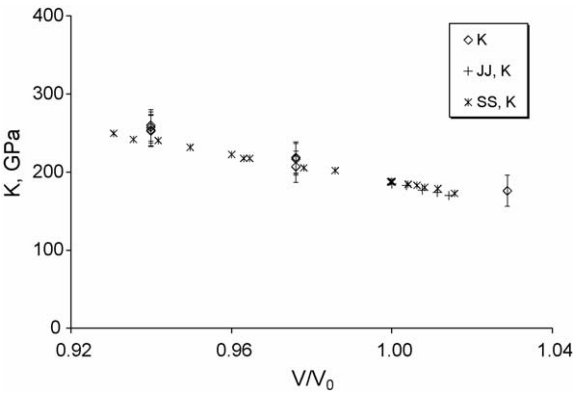

Fig. 3. Calculated bulk modulus (K) vs. volume (V/V_0) at high pressure and temperature (P–T). JJ represents data at elevated temperature–room pressure (Jackson et al., 2000); SS represents data at room-temperature—high pressure (Sinogeikin et al., 2003).

Table 3
Thermal expansion α and Grűneisen parameter γ at high pressure and temperature

T (K)	P_c (GPa)	V (Å^3)	α	$(\partial P/\partial T)_V$ (GPa K^{-1})	γ
1500	22.1(2)	493.04	1.99	0.00516	1.13
2000	24.7(3)	493.04	1.99		1.12
3000	29.8(4)	493.04	1.99		1.11
1500	13.3(3)	512.00	2.42	0.00525	1.19
2000	15.9(3)	512.00	2.42		1.18
3000	21.0(3)	512.00	2.42		1.17

Finally, we model the pressure–volume relationship with a third order Birch–Murnaghan equation of state. Since our calculations are mostly at high temperature (above the Debye temperature) and the Earth's mantle is also at high temperature, we define the reference condition for the equation of state as zero pressure and 2000 K. We fit the Reuss–Voigt–Hill averaged shear modulus with a third order Eulerian strain equation of state (Bina and Helffrich, 1992) given by

$$\mu = \mu_0(1 + 2f)^{5/2}\{1 - f[5 - 3(\partial\mu^0/\partial P)(K_0/\mu^0)]\} \quad (1)$$

where $f = (1/2)[(V_0/V)^{2/3} - 1]$ and μ^0 represents the 2000 K room pressure value of the shear modulus. The best fit is for μ^0 of 90.5 GPa and $\partial\mu^0/\partial P$ of 2.07. Table 4 summarizes all calculated thermoelastic properties at 2000 K and room pressure. These values allow us to calculate the thermoelasticity at relevant mantle pressures and temperatures. The finite strain equation of state allows us to interpolate between the pressures and temperatures of the VASP calculations.

The values in Table 4 are based on the high temperature, high pressure AIMD calculations with one adjustable parameter used to correct the pressure so as to yield the experimental room pressure volume. From the parameters in Table 4, we can calculate the properties along the geotherm where Mg_2SiO_4 ringwoodite is stable. We can also calculate these properties at P–T conditions for which experimental data have been reported.

Table 4
2000 K, room pressure thermoelastic properties of ringwoodite

Property	Value
V (Å^3)	560(3)
α (K^{-1})	3.85×10^{-5}
δ	5.2
γ	1.34
q	1.44
K_T^0 (GPa)	138(6)
$(\partial K_T/\partial P)_T$	5.2(3)
$(\partial K_T/\partial T)_V$ (GPa/K)	0
μ^0 (GPa)	90.5
$(\partial \mu/\partial P)_T$	2.07
$(\partial \mu/\partial T)_V$ (GPa/K)	−0.0086

A Birch–Murnaghan fitting of the AIMD bulk modulus vs. volume and corrected-pressure vs. volume yield these 2000 K reference volume state and bulk modulus variables. Shear modulus is derived from a third order Eulerian finite strain fit.

Li (2003) report room temperature P and S velocities to pressures up to 12 GPa; Sinogeikin et al. (2003) report single-crystal sound velocities at room temperature up to 17 GPa and room pressure at temperatures up to 650 °C, while Jackson et al. (2000) report such data to 600 °C. In Fig. 4 we illustrate the experimental measurements of aggregate acoustic velocities that have been deduced from these studies. The values of the velocities that are calculated using the parameters in Table 4 are illustrated by solid lines. Even though the experimental velocities were not used as constraints on the AIMD model, we see that the agreement is excellent. We thus expect that the AIMD calculations will provide excellent predictions of the acoustic velocities at P and T conditions along the geotherm where experimental data are not available.

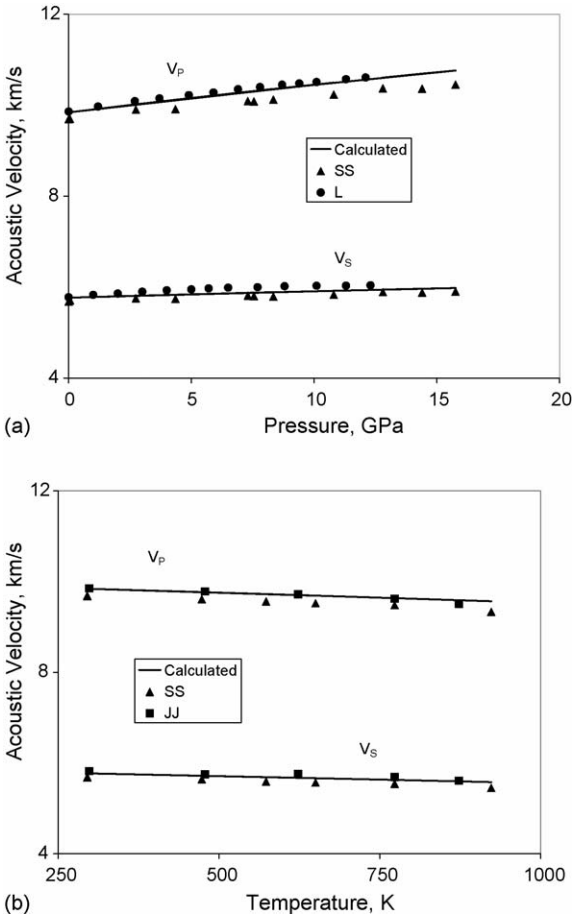

Fig. 4. Measured and calculated acoustic velocities as a function of P (a) and T (b). The curve labelled calculated are the values calculated from the properties in Table 4. The experimental data points labelled L are from Li (2003), SS is from Sinogeikin et al. (2003), and JJ is from Jackson et al. (2000).

5. Geophysical implications

One of the key variables for interpreting the seismic anisotropy (Deuss and Woodhouse, 2001; Fischer and Wiens, 1996; Montagner and Kennett, 1996; Revenaugh and Jordan, 1991; Shearer, 1990) is the elastic anisotropy of the minerals. Cubic materials require only one parameter, A, to express the elastic anisotropy. A is typically defined as the ratio of two shear moduli, c_{44} and $(1/2)(c_{11} - c_{12})$. The calculated value of A is 1.1 ± 0.1 in the calculated P–T range, and is compared with observations in Fig. 5. The elastic anisotropy decreases with volume in these calculations. Previous studies (Kiefer et al., 1997) have also shown that the elastic anisotropy of ringwoodite is small in the pressure range of 0–30 GPa. Table 5 lists the computed maximum and minimum P and S velocities at $T = 0$ K (for $V = 539.67$ Å^3), and $T = 2000$ K (for $V = 512.00$ and 493.04 Å^3). The direction

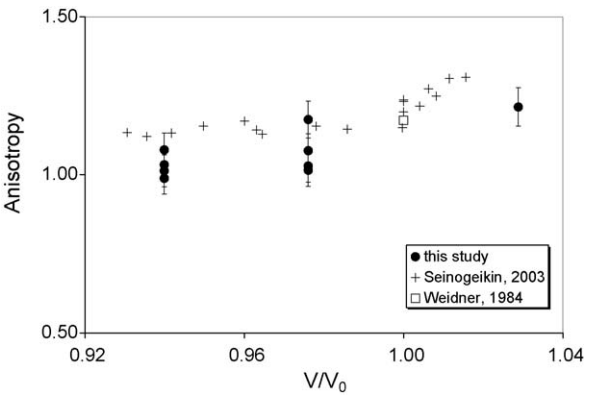

Fig. 5. Anisotropy $A = 2c_{44}/(c_{11} - c_{12})$ vs. (V/V_0).

Table 5
Computed maximum and minimum P and S velocities at $T = 0$ K (for $V = 539.67$ Å^3); and $T = 2000$ K (for $V = 512.00$ and 493.04 Å^3)

	$V = 539.67$ Å^3	$V = 512.00$ Å^3	$V = 493.04$ Å^3
V_{Pmax} (km s)	10.00	10.06	10.55
V_{Pmin} (km/s)	9.56	10.03	10.40
V_{Pmax}/V_{Pmin}	1.05	1.00	1.01
V_{Smax} (km/s)	6.07	5.67	5.75
V_{Smin} (km/s)	5.50	5.62	5.53
V_{Smax}/V_{Smin}	1.10	1.01	1.04
$(VSH/VSV)_{max}$	1.10	1.01	1.04

The propagation direction for maximum P wave velocity is (1 1 1), for minimum P velocity the direction is (1 0 0), the maximum S velocity propagates in the (1 0 0) direction with any polarization direction, the minimum S wave velocity is in the (1 1 0) direction polarized in the (1 −1 0) direction, as dictated by the cubic symmetry of ringwoodite.

for the maximum P wave velocity is (1 1 1); for the minimum P wave direction is (1 0 0); for the maximum S wave direction is (1 0 0) (polarized in the (0 1 0) direction); the minimum S wave direction is (1 1 0) (polarized in the (1 −1 0) direction); the maximum S wave anisotropy direction is (1 1 0) (polarized in the (1 −1 0) rather than (0 0 1) directions) as dictated by the cubic symmetry of ringwoodite. Our results, after taking the temperature into account, indicate that ringwoodite is remarkably isotropic at mantle *P–T* conditions. In contrast to olivine and other mantle minerals, ringwoodite will not provide a seismic signal of mantle flow.

Using the 1873 K (at 660 km depth) geotherm of Brown and Shankland (1981) we calculate the longitudinal and shear wave velocities for the magnesium end member of ringwoodite and compare these values to those of PREM (Dziewonski and Anderson, 1981) in Fig. 6. The pure magnesium ringwoodite is significantly

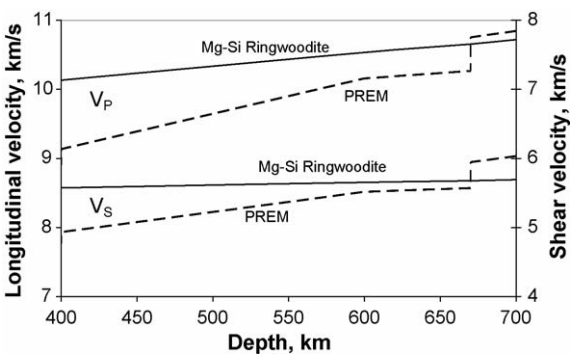

Fig. 6. Acoustic velocities for ringwoodite along a geotherm compared with PREM (Dziewonski and Anderson, 1981) in the transition zone. The geotherm is at 1873 K at 660 km depth with the gradient from Brown and Shankland (1981). Ringwoodite calculations are interpolated using a third order Eulerian finite strain model with the parameters given in Table 4.

faster than PREM in its stability field from 550–660 km depth. Indeed, both iron substitution for magnesium and the presence of garnet will lower the absolute velocities. However, the gradient induced by pressure in ringwoodite is much shallower than that for PREM for the entire transition zone. The origin of this steep gradient in PREM will be difficult to reconcile with models of uniform composition and phase over most of the transition zone.

Acknowledgements

This work is support by NERC (Grant Nos. NER/T/S/2001/00855; NER/O/S/2001/01227), and computer facilities provided by NERC at University College London, and the High Performance Computing Facilities of the University of Manchester (CSAR) and the Daresbury Laboratory (HPCx). DJW acknowledges the Leverhulme Trust for support through the visiting Professor program. DJW and LL acknowledge NSF EAR-9909266, EAR0135551, EAR00135550.

References

Alfè, D., 1999. Ab-initio molecular dynamics, a simple algorithm for charge extrapolation. Comput. Phys. Commun. 118, 31–33.
Allen, M.P., Tildesley, D.J., 1997. Computer Simulation of Liquids. Oxford University Press, New York, NY, USA, 408 pp.
Anderson, D.L., Bass, J.D., 1986. Transition region of the Earth's upper mantle. Nature 320, 321–328.
Bina, C.R., Helffrich, G.R., 1992. Calculation of elastic properties from thermodynamic equation of state principles. Ann. Rev. Earth Planet. Sci. 20, 527–552.
Blöchl, P.E., 1994. Projector augmented-wave method. Phys. Rev. B 50, 17953–17979.
Brown, J.M., Shankland, T.J., 1981. Thermodynamic parameters in the Earth as determined from seismic profiles. Geophys. J. Roy. Astronomy Soc. 66, 579–596.
Deuss, A., Woodhouse, J., 2001. Seismic observations of splitting of the mid-transition zone discontinuity in Earth's mantle. Science 294 (5541), 354–357.
Duffy, T.S., Anderson, D.L., 1989. Seismic velocities in mantle minerals and the mineralogy of the upper mantle. J. Geophys. Res. B: Solid Earth Planets 94, 1895–1912.
Dziewonski, A.M., Anderson, D.L., 1981. Preliminary reference Earth model. PEPI 25, 297–356.
Fischer, K.M., Wiens, D.A., 1996. The depth distribution of mantle anisotropy beneath the Tonga subduction cone. Earth Planet. Sci. Lett. 142, 253–260.
Jackson, J.M., Sinogeikin, S.V., Bass, J.D., Liebermann, R.C.E., Isaak, D.G.E., 2000. Sound velocities and elastic properties of gamma-Mg_2SiO_4 to 873 K by Brillouin spectroscopy. Am. Mineral. 85 (2), 296–303.
Karato, S.-I., 1998. Seismic anisotropy in the deep mantle, boundary layers and the geometry of mantle convection. Pure Appl. Geophys. 151 (2–4), 565–587.

Kavner, A., 2003. Elasticity and strength of hydrous ringwoodite at high pressure. Earth Planet. Sci. Lett. 214 (3/4), 645–654.

Kavner, A., Duffy, T.S., 2001. Strength and elasticity of ringwoodite at upper mantle pressures. Geophys. Res. Lett. 28 (14), 2691–2694.

Kiefer, B., Stixrude, L., Wentzovitch, R.M., 1997. Calculated elastic constants and anisotropy of Mg_2SiO_4 spinel at high pressure. Geophys. Res. Lett. 24 (22), 2841–2844.

Kresse, G., Furthmüller, J., 1996. Efficient iterative schemes for ab initio total-energy calculations using a plane-wave basis set. Phys. Rev. B 54, 11169.

Kresse, G., Joubert, D., 1999. From ultrasoft pseudopotentials to the projector augmented-wave method. Phys. Rev. B 59, 1758–1775.

Li, B., 2003. Compressional and shear wave velocities of ringwoodite gamma-Mg_2SiO_4 to 12 GPa. Am. Mineral. 88, 1312–1317.

Li, L., et al. Elasticity of $CaSiO_3$ perovskite at high pressure and high temperature, PEPI, submitted for publication.

Matsui, M., 1999. Computer simulation of the Mg (sub 2) SiO (sub 4) phases with application to the 410 km seismic discontinuity. PEPI 116 (1–4), 9–18.

Meng, Y., et al., 1993. In situ high *P-T* X-ray diffraction studies on three polymorphs (alpha, beta, gamma) of Mg (sub 2) SiO (sub 4). J. Geophys. Res. B: Solid Earth Planets 98 (12), 22,199–22,207.

Montagner, J.P., Kennett, B.L.N., 1996. How to reconcile body-wave and normal mode-reference earth models. Geophys. J. Int. 125, 229–248.

Nye, J.F., 1957. Physical Properties of Crystals. Oxford University Press, Ely House, London.

Oganov, A.R., Brodholt, J.P., Price, G.D., 2001a. Ab initio elasticity and thermal equation of state of $MgSiO_3$ perovskite. Earth Planet. Sci. Lett. 184 (3/4), 555–560.

Oganov, A.R., Brodholt, J.P., Price, G.D., 2001b. The elastic constants of $MgSiO_3$ perovskite at pressures and temperatures of the Earth's mantle. Nature (London) 411 (6840), 934–937.

Revenaugh, J., Jordan, T.H., 1991. The ScS phase in the reflection of S-waves from the core-mantle boundary. J. Geophys. Res. Solid Earth 96 (19736).

Rigden, S.M., Gwanmesia, G.D., Fitz Gerald, J.D., Jackson, I., Liebermann, R.C., 1991. Spinel elasticity and seismic structure of the transition zone of the mantle. Nature (London) 354 (6349), 143–145.

Sasaki, S., Prewitt, C.T., Sato, Y., Ito, E., 1982. Single-crystal X-ray study of gamma Mg_2SiO_4. J. Geophys. Res. 87 (B9), 7829–7832.

Shearer, P.M., 1990. Seismic imaging of upper-mantle strucutre with new evidence for a 520-km discontinuity. Nature (London) 344 (6262), 121–126.

Sinogeikin, S.V., Bass, J.D., Katsura, T., 2001. Single-crystal elasticity of gamma-$(Mg_{0.91}Fe_{0.09})_2SiO_4$ to high pressures and to high temperatures. Geophys. Res. Lett. 28 (22), 4335–4338.

Sinogeikin, S.V., Bass, J.D., Katsura, T., 2003. Single-crystal elasticity of ringwoodite to high pressures and high temperatures; implications for 520 km seismic discontinuity. PEPI 136 (1/2), 41–66.

Stackhouse, S., Brodholt, J.P., Wookey, J., Kendall, J.-M., Price, G.D., 2004. The effect of temperature on the seismic anisotropy of the perovskite and post-perovskite polymorphs of $MgSiO_3$. Earth Planet. Sci. Lett. 230 (1–2), 1–10.

Weidner, D.J., Li, L., Davis, M., Chen, J., 2004. Effect of plasticity on elastic modulus measurements. Geophys. Rev. Lett. 31 (6), 19090.

Weidner, D.J., Sawamoto, H., Sasaki, S., 1984. Single-crystal elastic properties of the spinel phase of Mg_2SiO_4. J. Geophys. Res. 89 (B9), 7852–7860.